J Mol Model (2012) 18:3427–3438
DOI 10.1007/s00894-012-1353-z

ORIGINAL PAPER

Does $Al_4H_{14}^-$ cluster anion exist? High-level *ab initio* study

Jerzy Moc

Received: 8 September 2011 / Accepted: 3 January 2012 / Published online: 27 January 2012

Abstract A comprehensive *ab initio* investigation using coupled cluster theory with the aug-cc-pVnZ, n=D,T basis sets is carried out to identify distinct structures of the $Al_4H_{14}^-$ cluster anion and to evaluate its fragmentation stability. Both thermodynamic and mechanistic aspects of the fragmentation reactions are studied. The observation of this so far the most hydrogenated aluminum tetramer was reported in the recent mass spectrometry study of Li et al. (2010) J Chem Phys 132:241103–241104. The four $Al_4H_{14}^-$ anion structures found are chain-like with the multiple-coordinate Al center and can be viewed approximately as comprising $Al_2H_7^-$ and Al_2H_7 moieties. Locating computationally some of the $Al_4H_{14}^-$ minima on the correlated *ab initio* potential energy surfaces required the triple-zeta quality basis set to describe adequately the Al multi-coordinate bonding. For the two most stable $Al_4H_{14}^-$ isomers, the mechanism of their low-barrier interconversion is described. The dissociation of $Al_4H_{14}^-$ into the $Al_2H_7^-$ and Al_2H_7 units is predicted to require 20-22 (10-13) kcal mol^{-1} in terms of ΔH (ΔG) estimated at T=298.15 K and p=1 atm. However, $Al_4H_{14}^-$ is found to be a metastable species in the gas phase: the H_2 loss from the radical moiety of its most favorable isomer is exothermic by 18 kcal mol^{-1} in terms of ΔH (298.15 K) and by 25 kcal mol^{-1} in terms of ΔG(298.15 K), with the enthalpic/free energy barrier involved being less than 1 kcal mol^{-1}. By contrast with alane $Al_4H_{14}^-$, only a weakly bound complex between $Ga_4H_{12}^-$ and H_2 has been identified for the gallium analogue using the relativistic effective core potential.

J. Moc (✉)
Faculty of Chemistry, Wroclaw University,
F. Joliot-Curie 14,
50-383, Wroclaw, Poland
e-mail: jerzy.moc@chem.uni.wroc.pl

Keywords $Al_4H_{14}^-$ and $Ga_4H_{14}^-$ hydrogen-rich clusters · Coupled cluster calculations · Potential energy surfaces · Thermodynamic and kinetic stability

Introduction

Aluminum-hydrides, or alanes, have been proposed to be potential hydrogen storage media, building blocks for new cluster assemblies and high-energy-density materials [1–6]. During the last three years, several novel alanes, both neutral and anionic, have been made and characterized. The emerging structural and electronic properties of alanes and their derivatives involving a small Al_4 cluster core have been notably the focus of the widespread interest [1, 2, 5, 6].

The new hydrogenated Al_4H_6 neutral cluster was reported to be a stable species in the gas phase based on the results of the photoelectron study of the corresponding anion $Al_4H_6^-$ and density functional theory (DFT) electronic structure calculations for the neutral [1]. Furthermore, the Al_4H_6 cluster was suggested to be a high-energy density molecule, with the estimated heat of combustion (giving the Al_2O_3 and water products) to be about 2.5 times greater than that for methane [1]. Various Al_4R_6 and Al_4R_5X derivatives of Al_4H_6 with the hydrogen atoms substituted by the bulky R groups and halogens X (R=P^tBu_2; X=Br,Cl) were subsequently prepared and structurally characterized [5].

The whole series of novel aluminum-hydride cluster anions $Al_4H_n^-$ were generated using the laser-induced plasma technique and characterized by mass spectrometry [2]. The most hydrogenated anionic aluminum tetramer reported in Ref. [2] was $Al_4H_{13}^-$. In the related study published recently, the new gas phase $Al_nH_m^-$ clusters were produced with a pulsed arc discharge source and identified using mass spectrometry [6]. The latter investigation reported the

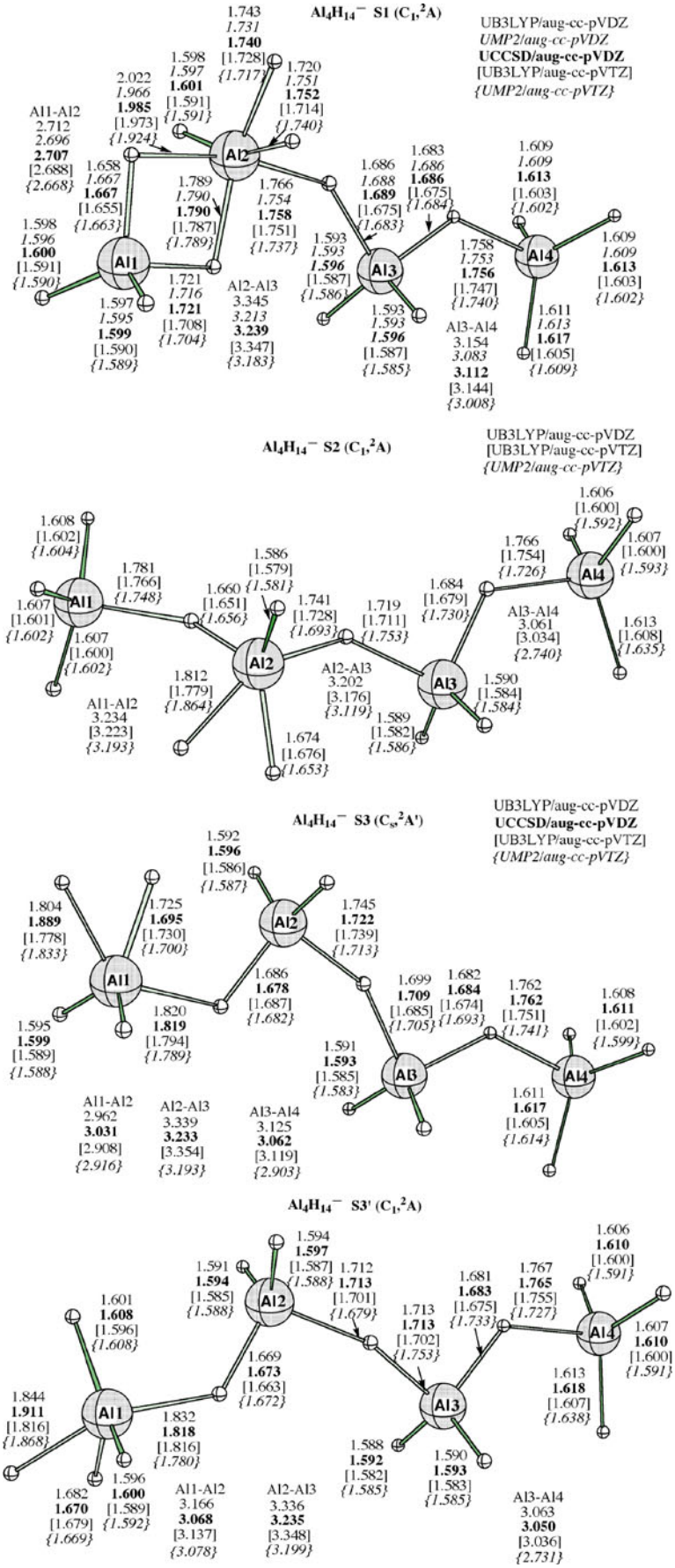

Fig. 1 **S1, S2, S3 and S3′** structures of the $Al_4H_{14}^-$ anion (distances in Ångstroms) calculated with the correlated *ab initio* and density functional methods using the aug-cc-pVnZ, n=D,T basis sets. Note that **S2** minimum has not been located on the UCCSD/aug-cc-pVDZ and UMP2/aug-cc-pVDZ potential energy surfaces, whereas **S3(S3′)** minima have not been identified on the UMP2/aug-cc-pVDZ energy surface (see the text)

Table 1 Relative energies (kcal mol^{-1}) of the **S1**, **S2**, **S3** and **S3′** structures of $Al_4H_{14}^-$ from the various theoretical methods[a]

Structure	aug-cc-pVDZ[b]			aug-cc-pVTZ[c]		
	UB3LYP	UMP2	UCCSD	UB3LYP	UMP2	UCCSD(T)
S1(C_1, ^2A)	0.0	0.0	0.0	0.0	0.0	0.0 (0.0)[e]
S2(C_1, ^2A)	−1.1	[d]	[d]	−0.6	1.2	0.0 (0.5)[e]
S3(C_s, $^2A'$)	−3.4	[d]	−4.0	−3.2	−2.1	−2.2 (-1.9)[e]
S3′(C_1, ^2A)	−3.3	[d]	−4.1	−2.8	−2.0	−1.8 (-1.3)[e]

[a] All values have been corrected for the zero-point vibrational energies

[b] At the geometries calculated with each method

[c] At the geometries calculated with each method, except for the UCCSD(T) value calculated at the UMP2/aug-cc-pVTZ optimized structure

[d] The structure has not been found at this level (see the text)

[e] In parentheses, G4(0 K) results are given

aluminum hydride clusters having an extraordinary hydrogen content, with the hydrogen atom number (m)-aluminum atom number (n) ratio exceeding 3: for n=5-8, the clusters with m=3n+1 hydrogen atoms were detected. Most notably, for n=4, the cluster having m=3n+2 hydrogens, or $Al_4H_{14}^-$, was observed according to the authors [6],

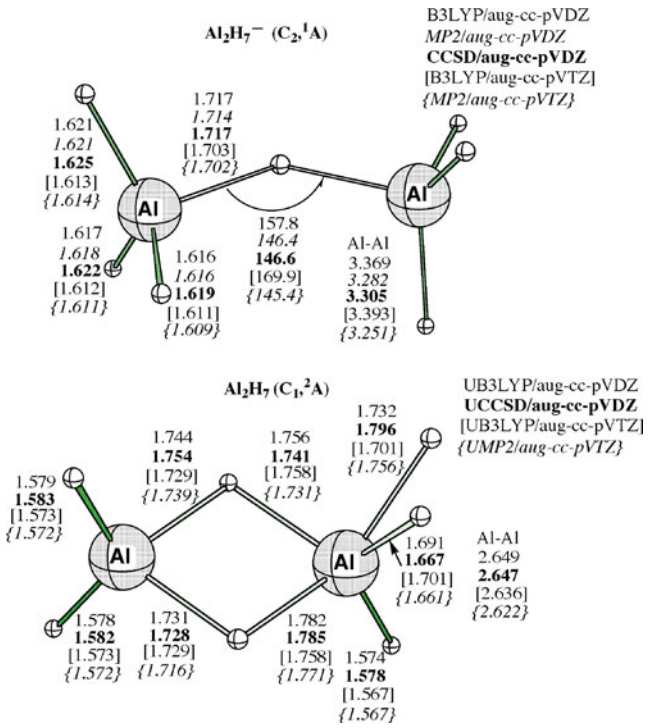

Fig. 2 Structures of the isolated $Al_2H_7^-$ anion and Al_2H_7 neutral (distances in Ångstroms) calculated with the correlated *ab initio* and density functional methods using the aug-cc-pVnZ, n=D,T basis sets. Note that Al_2H_7 minimum has not been located on the UMP2/aug-cc-pVDZ potential energy surface

although the actual structure of this cluster anion with an open electronic shell was not reported.

Previously, using density functional and correlated *ab initio* methods we compared the structures, thermodynamic stabilities and bonding of the multiply hydrogenated aluminum and gallium neutral clusters M_3H_9 and M_4H_{12} (M=Al, Ga) [7]. The distinct difference found between the corresponding clusters with M=Al and Ga was the stability of the open type structures called by us "hypervalent", involving the five- or six-coordinate M atom (in terms of the M-H bonds). We showed specifically that, for M=Al, such a structure was relatively stable, lying within 2 kcal mol^{-1} of the cyclic global minimum, whereas for M=Ga, the "hypervalent" isomer appeared to be destabilized relative to the lowest energy cyclic species, especially for M_4H_{12} [7].

Herein we present extensive high-level *ab initio* calculations of the structures and fragmentation stability of $Al_4H_{14}^-$ as well as of the reaction paths for interconversion and decomposition of the anion. Notably, for this novel species, we have carefully studied the dependence of the calculated results on the level of theory used. As described below, we have identified four different chain-like structures of $Al_4H_{14}^-$ which involve the multiple-coordinate Al center, reminiscent of the structural motif seen in the "hypervalent" isomer of the Al_4H_{12} cluster [7]. In order to assist in the future assignment of the actual isomer of the $Al_4H_{14}^-$ anion present in the experimental mass spectrum [6], we have calculated vertical electron detachment energies (VDEs) for the distinct structures. We also show that by contrast to the aluminum hydride $Al_4H_{14}^-$, only a weakly bound complex between the $Ga_4H_{12}^-$ anion and H_2 has been identified for the gallium counterpart $Ga_4H_{14}^-$.

Computational methods

Coupled cluster theory with single and double excitations (CCSD) [8] and second-order Møller-Plesset perturbation theory (MP2) [9] were used in conjunction with the augmented correlation consistent aug-cc-pVnZ, n=D,T basis sets [10, 11]. All the geometries were optimized and characterized as minima or relevant transition states at each computational level. The MP2 vibrational frequencies were calculated using the analytical Hessians, whereas the CCSD frequencies were computed with the analytical gradients and numerical Hessians. For comparison, optimizations and frequency calculations were also carried out using the same basis sets with the B3LYP density functional [12, 13]. Spin-unrestricted (U) version of each method was used for the open-shell species. To establish accurate energetics, single-point energy calculations were performed at the MP2/aug-cc-pVTZ geometries using CCSD with perturbatively included triples (CCSD(T)) [8] with the aug-cc-pVTZ basis

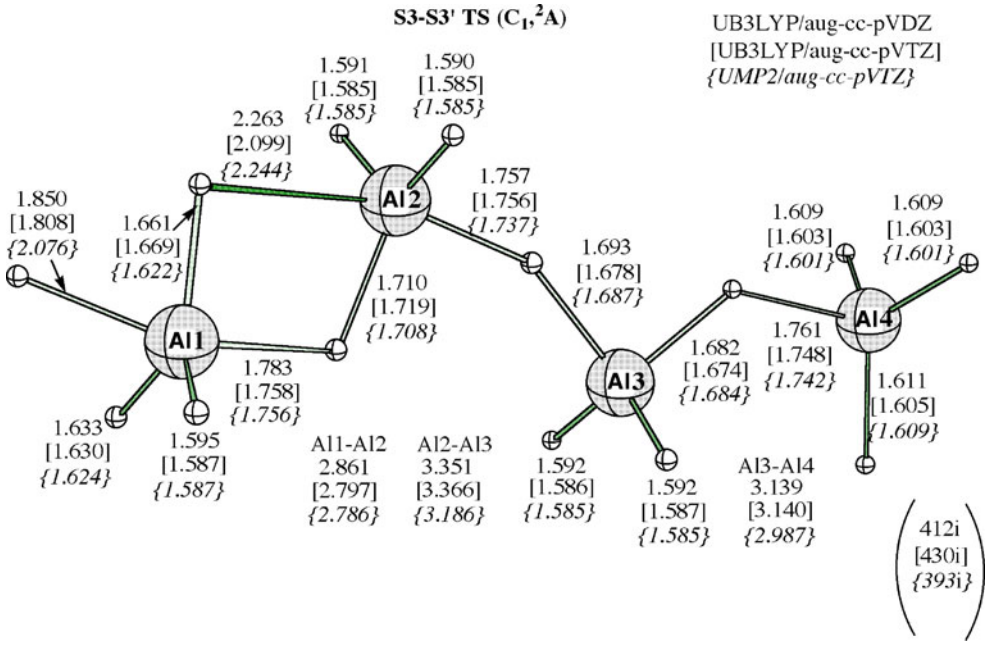

Fig. 3 A structure of the transition state **S3-S3′ TS** (distances in Ångstroms) calculated with the correlated *ab initio* and density functional methods using the aug-cc-pVnZ, n=D,T basis sets. **S3-S3′ TS** is a saddle point for the $Al_4H_{14}^-$ (**S3**) → $Al_4H_{14}^-$ (**S3′**) interconversion (cf. Fig. 4); the associated imaginary frequency is given at each computational level

set [10, 11]. In addition, the structures and stability of $Al_4H_{14}^-$ were studied using the multi-level G4 scheme [14]. Enthalpies and Gibbs free energies were calculated at T=298.15 K and p=1 atm. For the gallium analogue, $Ga_4H_{14}^-$, the energy-consistent effective core potential (ECP), ECP10MDF [15], which replaces the $1s^22s^22p^6$ core of Ga by the pseudopotential was used (in addition to the all-electron calculations) to take into account relativistic effects of this atom. The explicitly treated Ga electrons ($3s^23p^63d^{10}4s^24p^1$) were described by the associated (11s12p10d2f)/[6s6p5d2f] basis set [16], augmented by diffuse functions (aug-cc-pVTZ-PP). The latter basis was employed in conjunction with the all-electron aug-cc-pVTZ basis sets for H [10, 11, 17]. The relevant computational methods using the ECP10MDF will be referred to as MP2/ECP and B3LYP/ECP. Calculations in the current work were performed employing Gaussian 09 program [18].

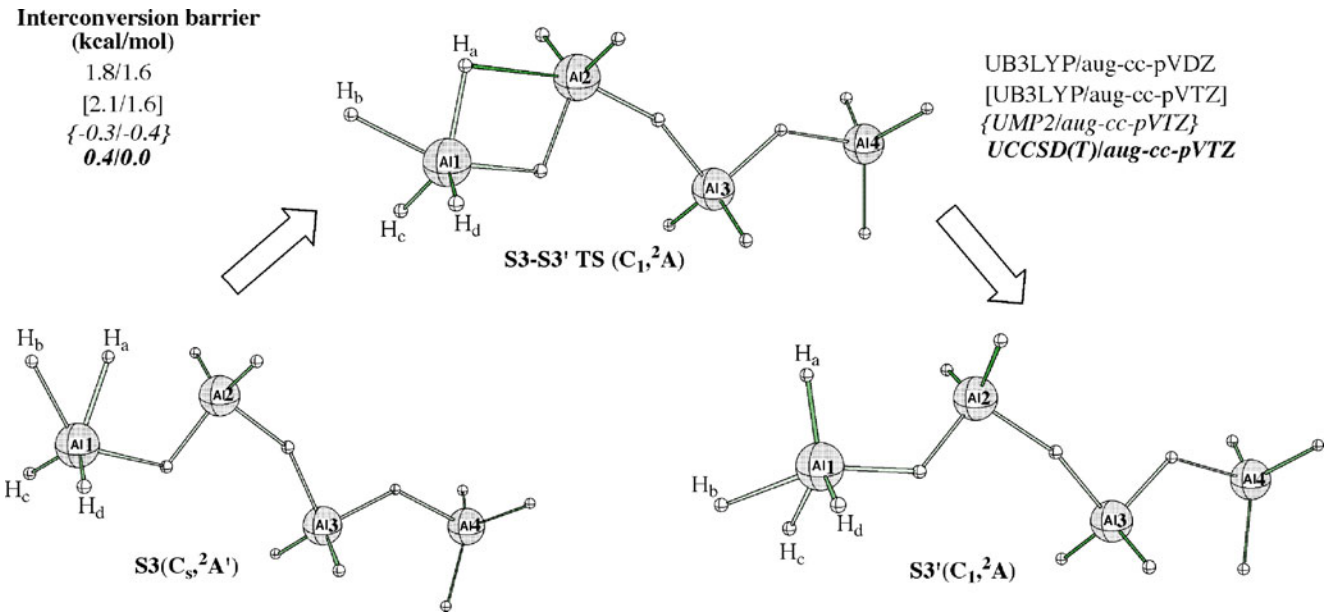

Fig. 4 Illustration of the $Al_4H_{14}^-$ (**S3**) → $Al_4H_{14}^-$ (**S3′**) interconversion occurring through the transition state **S3-S3′ TS**. The interconversion barrier values shown have been corrected for the zero-point vibrational energies; the value before (after) slash is for the **S3→S3′** (**S3′→S3**) rearrangement

Table 2 Energies of unimolecular fragmentation reactions (kcal mol^{-1}) of $Al_4H_{14}^-$ from the various theoretical methods[a]

Fragmentation channel	aug-cc-pVDZ[b]			aug-cc-pVTZ[c]		
	UB3LYP	UMP2	UCCSD	UB3LYP	UMP2	UCCSD(T)
S1→$Al_2H_7^-$+Al_2H_7	15.4	12.7	18.1	15.2	19.6	19.7 (20.5)[e]
S2→$Al_2H_7^-$+Al_2H_7	16.5	[d]	[d]	15.8	19.6	19.7 (20.0)[e]
S3→$Al_2H_7^-$+Al_2H_7	18.8	[d]	22.1	18.4	21.7	21.9 (22.4)[d]
S3′→$Al_2H_7^-$+Al_2H_7	18.7	[d]	22.2	18.0	21.5	21.5 (21.8)[d]
S1→$Al_4H_{13}^-$+H	−0.7	−8.5	−6.5	0.3	−5.6	−2.4 (-1.3)[e]
S2→$Al_4H_{13}^-$+H	0.4	[d]	[d]	0.9	−5.6	−2.4 (-1.8)[e]
S3→$Al_4H_{13}^-$+H	2.7	[d]	−2.5	3.6	−3.6	−0.2 (0.6)[e]
S3′→$Al_4H_{13}^-$+H	2.5	[d]	−2.5	3.1	−3.7	−0.6 (0.0)[e]
S1→$Al_4H_{12}^-$+H_2	−20.0	−23.5	−24.0	−20.7	−23.3	−22.3 (-21.1)[e]
S2→$Al_4H_{12}^-$+H_2	−18.9	[d]	[d]	−20.1	−23.2	−22.3 (-21.7)[e]
S3→$Al_4H_{12}^-$+H_2	−16.6	[d]	−20.1	−17.5	−21.2	−20.0 (-19.2)[e]
S3′→$Al_4H_{12}^-$+H_2	−16.7	[d]	−20.0	−17.9	−21.3	−20.4 (-19.8)[e]

[a] All values have been corrected for the zero-point vibrational energies. A positive (negative) sign indicates that $Al_4H_{14}^-$ is thermodynamically stable (unstable) relative to the fragmentation products

[b] At the geometries calculated with each method

[c] At the geometries calculated with each method, except for the UCCSD(T) value calculated at the UMP2/aug-cc-pVTZ optimized structures

[d] The $Al_4H_{14}^-$ structure has not been found at this level (see the text)

[e] In parentheses, G4(0 K) results are given

Results and discussion

$Al_4H_{14}^-$ structures - method dependence

Figure 1 illustrates the optimization level dependence of the four distinct structures of the $Al_4H_{14}^-$ cluster anion, **S1**(^{2}A), **S2**(^{2}A), **S3**(^{2}A′) and **S3′**(^{2}A). These doublet structures are chain-like with the bridging hydrogens. Attempts to locate a cyclic $Al_4H_{14}^-$ isomer were unsuccessful. Computations show that **S1** exists on the potential energy surfaces calculated at the five levels (with all positive force constants predicted at each level). By contrast, the identification of **S2** appeared to be method dependent: this structure has been located on the UB3LYP/aug-cc-pVDZ, UB3LYP/aug-cc-pVTZ and UMP2/aug-cc-pVTZ potential energy surfaces, but not on the UMP2/aug-cc-pVDZ and UCCSD/aug-cc-pVDZ surfaces. In turn, **S3** and **S3′** structures are potential minima at all the levels, but UMP2/aug-cc-pVDZ. These results indicate that with the correlated methods, the triple-zeta flexibility basis set is required to describe adequately the bonding situation for $Al_4H_{14}^-$.

Table 3 Thermodynamic values of unimolecular fragmentation reactions (kcal mol^{-1}) of $Al_4H_{14}^-$ calculated at the G4 level[a]

Fragmentation channel	ΔH (298.15 K)[b]	ΔG(298.15 K)[c]
S1→$Al_2H_7^-$+Al_2H_7	20.7	10.1
S2→$Al_2H_7^-$+Al_2H_7	19.6	10.1
S3→$Al_2H_7^-$+Al_2H_7	22.3	13.0
S3′→$Al_2H_7^-$+Al_2H_7	21.5	13.0
S1→$Al_4H_{13}^-$+H	0.0	−7.3
S2→$Al_4H_{13}^-$+H	−1.1	−7.3
S3→$Al_4H_{13}^-$+H	1.6	−4.4
S3′→$Al_4H_{13}^-$+H	0.8	−4.4
S1→$Al_4H_{12}^-$+H_2	−19.4	−27.7
S2→$Al_4H_{12}^-$+H_2	−20.5	−27.7
S3→$Al_4H_{12}^-$+H_2	−17.8	−24.9
S3′→$Al_4H_{12}^-$+H_2	−18.7	−24.8

[a] A positive (negative) sign indicates that $Al_4H_{14}^-$ is thermodynamically stable (unstable) relative to the fragmentation products

[b] ΔH (298.15 K) enthalpies and ΔG(298.15 K) free energies were calculated at the 1 atm and 298.15 K using the vibrational frequencies evaluated at the UB3LYP/GTBas3 level [14]

As seen in Fig. 1, the unique features of the $Al_4H_{14}^-$ species are the involvement of the multi-coordinate (Al1 or Al2) atom, the presence of not symmetrical Al-H-Al bridges with the H atoms not shared equally with the Al atoms as well as the presence of the significantly elongated terminal Al1(Al2)-H bonds. It is relevant to note here that multi-coordinate Al centers (participating in the six Al-H-Al bridges) were first observed in the solid state structure of AlH_3 polymer in 1969 [19].

Figure 1 also shows that the use of the correlated methods, especially in conjunction with the aug-cc-pVTZ basis set, causes a significant shortening of most of the Al-Al distances (up to 0.3 Å) along with a major decrease of the Al2-H

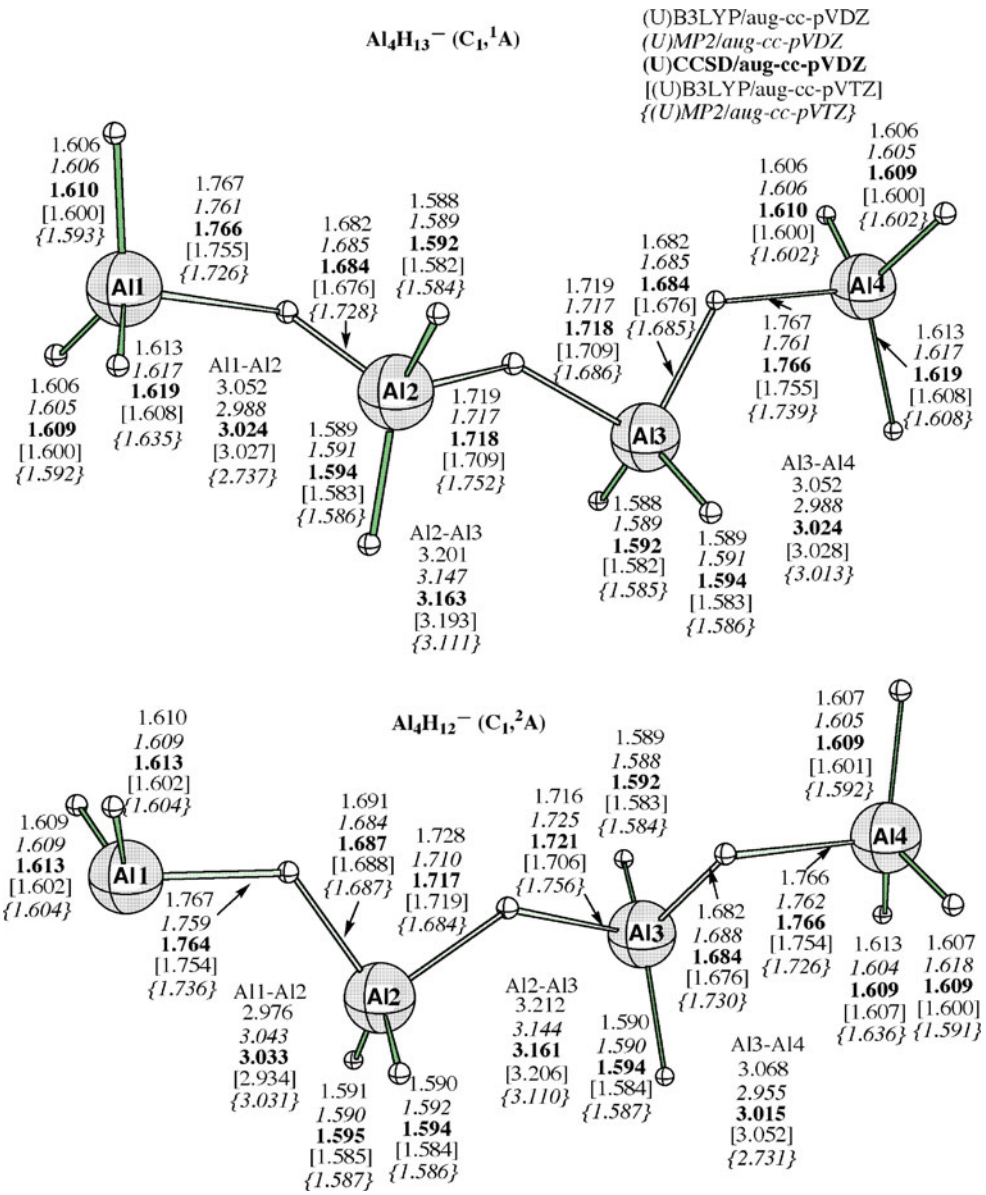

Fig. 5 Structures of the $Al_4H_{13}^-$ and $Al_4H_{12}^-$ anions (distances in Ångstroms), being the products of H and H_2 loss from $Al_4H_{14}^-$, respectively, calculated with the correlated *ab initio* and density functional methods using the aug-cc-pVnZ, n=D,T basis sets

bridging bond of **S1** (relative to the UB3LYP results). As the energy calculations indicate (see Table 1), the four $Al_4H_{14}^-$ species are of similar stability, lying within 2.2 and 2.4 kcal mol^{-1} at the most comprehensive UCCSD(T)/aug-cc-pVTZ//UMP2/aug-cc-pVTZ and G4 (0 K) levels, respectively, with **S3** being the most stable of the four, followed by **S3′**.

We suggest that the simplest description of the $Al_4H_{14}^-$ anion structure would involve the '$Al_2H_7^-$' and 'Al_2H_7' units. To support this model we report in Fig. 2 the optimized geometries of the isolated $Al_2H_7^-$ anion and Al_2H_7 radical (both structures in Fig. 2 show positive force constants at each computational level). We find further support from the Mulliken spin populations, which indicate that the 'Al_2H_7' fragment of **S1** and **S3**(**S3′**) is a sole carrier of the spin density. For **S2**, although its neutral fragment differs most from the isolated Al_2H_7 geometry (the former matches rather the higher energy Al_2H_7 isomer [20]), similar to the cases of **S1** and **S3**(**S3′**), this moiety holds the spin density.

The results in Fig. 2 further show that an appreciable bending occurs for isolated $Al_2H_7^-$ at the correlated levels compared to the UB3LYP results. Earlier computational studies of $Al_2H_7^-$ established this anion to be thermodynamically stable with respect to both the $AlH_3+AlH_4^-$ [21] and $Al_2H_6+H^-$ [22, 23] fragmentations. For isolated $Al_2H_7(^2A)$, we predicted the lowest energy structure to be double-bridged, in agreement with the recent density functional work [20] (note that with UB3LYP/aug-cc-pVTZ, Al_2H_7 has higher C_s ($^2A''$) symmetry). This radical species also features two lengthened terminal Al-H bonds, to 1.66 and 1.76 Å, with a relatively short Al-Al distance of 2.62 Å (the UMP2/aug-cc-pVTZ results), and it bears resemblance with the radical moiety of $Al_4H_{14}^-$, especially for **S1**. The adiabatic

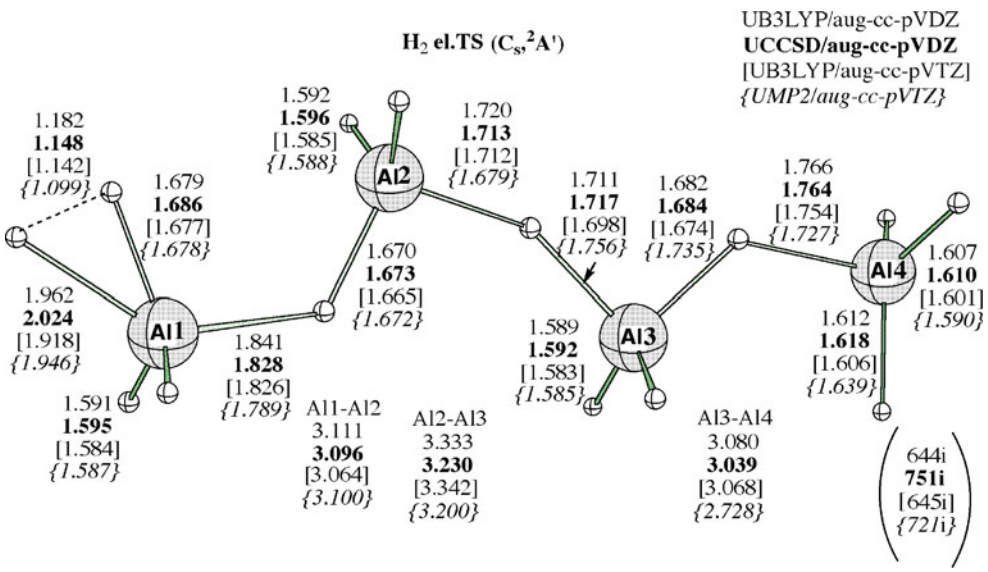

Fig. 6 A structure of the transition state **H_2el. TS** for H_2 elimination from $Al_4H_{14}^-$ (**S_3**) (distances in Ångstroms), calculated with the correlated *ab initio* and density functional methods using the aug-cc-pVnZ, n=D,T basis sets; the associated imaginary frequency is given at each computational level

electron detachment energy of the $Al_2H_7^-$ anion, or the adiabatic electron affinity of the Al_2H_7 neutral was computed to be relatively high at 4.14 (4.20) eV with the UCCSD(T)/aug-cc-pVTZ//UMP2/aug-cc-pVTZ (G4 (0 K)) calculations, pointing to the appreciable electronic stability of the anion.

Interconversion of $Al_4H_{14}^-$ isomers

We found that the lowest-energy isomers of $Al_4H_{14}^-$, **S3** and **S3′**, are connected by the transition state **S3-S3′ TS**, shown in Fig. 3. During this interconversion, H_a and H_b of **S3** move in the opposite directions, breaking C_s symmetry

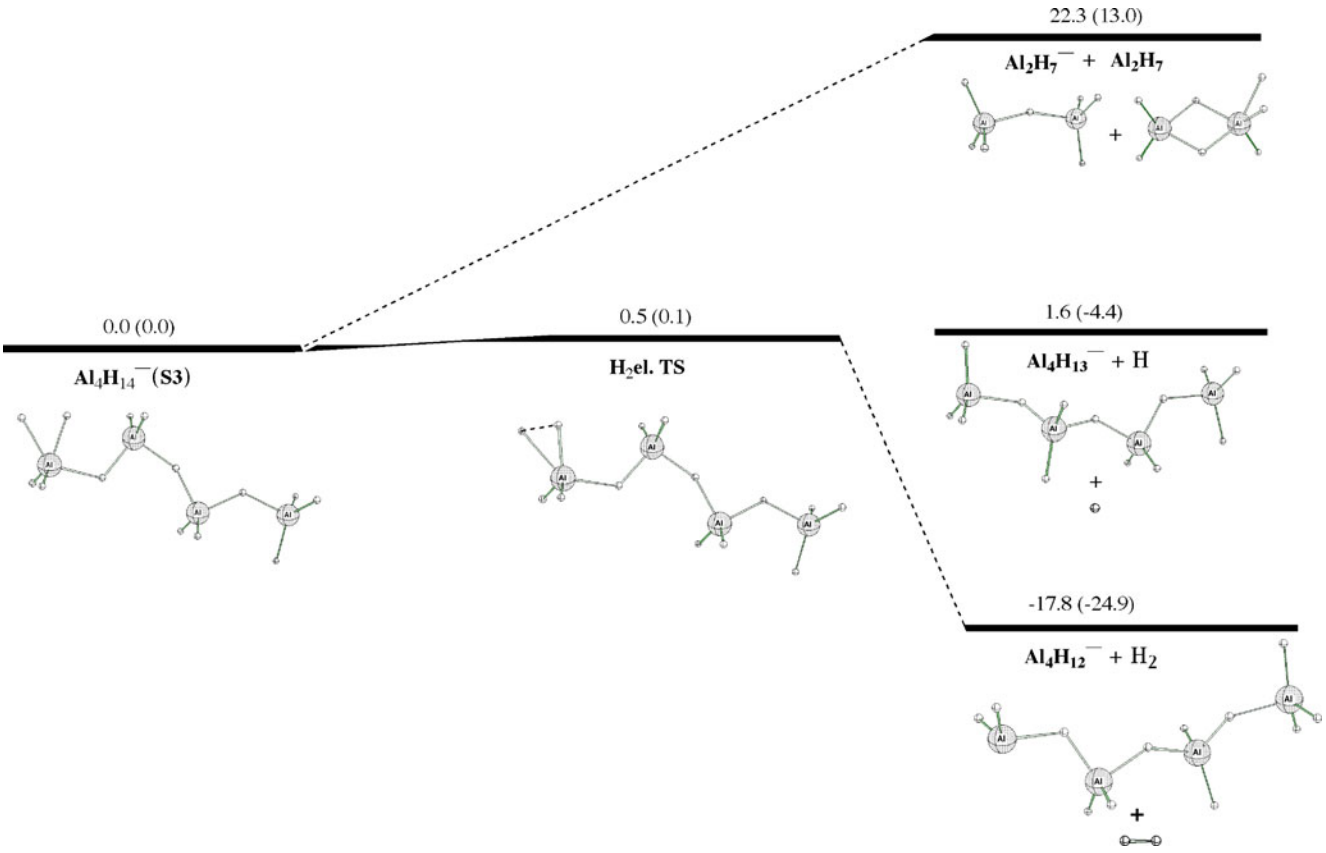

Fig. 7 Schematic profiles of ΔH (298.15 K) for the three fragmentation channels of the $Al_4H_{14}^-$ (**S3**) anion (in kcal mol^{-1}); the corresponding ΔG (298.15 K) values are given in parentheses (G4 results). Note that the $Al_4H_{12}^-$…H_2 post-reaction complex (shown in Fig. 8) has been omitted in the H_2 elimination path

(see Fig. 4). Past the **S3-S3′ TS**, H_b keeps moving toward H_c, whereas H_a moves away from Al2. In the resulting **S3′** structure of very similar stability to **S3** (Table 1), the new longest terminal Al1-H links are those involving H_b and H_c of 1.67 and 1.87 Å (the UMP2/aug-cc-pVTZ results), with H_a forming "normal" terminal bond, similar to H_d. The **S3 → S3-S3′ TS → S3′** reaction path is confirmed by the intrinsic reaction coordinate (IRC) computation. At the UCCSD(T)/aug-cc-pVTZ level, only a tiny barrier for the **S3 → S3′** rearrangement is predicted of 0.4 kcal mol^{-1} (note that in the reverse direction, the barrier does not exist at this level, see the upper left panel in Fig. 4).

Fragmentation stability of $Al_4H_{14}^-$

We next assessed the fragmentation stability of the $Al_4H_{14}^-$ anion. The computed energies of the fragmentation reactions of the four isomers of $Al_4H_{14}^-$ are reported in Table 2, while the corresponding thermodynamic values are given in Table 3. We have considered three unimolecular decomposition channels: (1) $Al_4H_{14}^- \rightarrow Al_2H_7^- + Al_2H_7$, (2) $Al_4H_{14}^- \rightarrow Al_4H_{13}^- + H$ and (3) $Al_4H_{14}^- \rightarrow Al_4H_{12}^- + H_2$. The choice of decomposition (1) is justified by the $Al_4H_{14}^-$ anion "bonding model" proposed above. The H loss reaction (2) affords the closed-shell anion $Al_4H_{13}^-$, observed in the gas phase by two research groups [2, 6], which is indicative of a relatively stable species. With the fragmentation channel (3) we examine if $Al_4H_{14}^-$ is stable with respect to loss of H_2 molecule of significant stability.

The last column of Table 2 which compares our most extended zero-point energy corrected UCCSD(T)/aug-cc-pVTZ//UMP2/aug-cc-pVTZ reaction energies with the G4 (0 K) values (the latter are given in parentheses) shows a very good agreement between both kinds of results. Therefore, the enthalpies ΔH (298.15 K) and free energies ΔG (298.15 K) presented in Table 3 and discussed in this section were estimated at the G4 level. Regarding decomposition (1), Table 3 indicates that this reaction is always endothermic, by 19.6-22.3 (10.1-13.0) kcal mol^{-1} with ΔH (298.15 K) (ΔG(298.15 K)). With respect to the H loss reaction (2) and in terms of ΔH (298.15 K), we found it to be slightly endothermic for **S3**, essentially thermoneutral for **S1** and **S3′** and insignificantly exothermic for **S2**. With ΔG (298.15 K), this reaction is moderately exothermic for all the $Al_4H_{14}^-$ species, by 4.4-7.3 kcal mol^{-1}. Note that the calculated chain-like structure of the $Al_4H_{13}^-$ decomposition product for reaction (2) is reported in the upper panel in Fig. 5. The alternative $Al_4H_{13} + H^-$ dissociation process is energetically much less favorable, by about 90 kcal mol^{-1}. This is explained by the considerably smaller electron affinity of H compared to Al_4H_{13}, 0.9 vs. 4.8 eV.

By contrast with the two former fragmentations, the reaction of H_2 elimination from $Al_4H_{14}^-$ (decomposition (3)) is found to be significantly exothermic, by 17.8-20.5 kcal mol^{-1} in terms of ΔH(298.15 K) and by 24.8-27.7 kcal mol^{-1} in terms of ΔG(298.15 K) (Table 3). These results indicate that the $Al_4H_{14}^-$ anion is thermodynamically disfavored. The structure of the corresponding dehydrogenation product, $Al_4H_{12}^-$, is shown in the lower panel in Fig. 5. In the next section we are reporting the related dehydrogenation pathway.

Reaction pathway for H_2 elimination from $Al_4H_{14}^-$ (S3)

The results of the previous section showed clearly that H_2 elimination from $Al_4H_{14}^-$ is by far the most thermodynamically favorable unimolecular decomposition of this anion. To assess kinetic stability of $Al_4H_{14}^-$, we have calculated the reaction pathway for H_2 loss occurring from the lowest energy **S3** isomer. Due to the proximity of H_a and H_b in $Al_4H_{14}^-$ (**S3**) (cf. Fig. 4), it is anticipated that the H_2 elimination will occur relatively easily from its radical moiety. Computations confirm this assumption. The $Al_4H_{14}^-$ (**S3**) → $Al_4H_{12}^- + H_2$ reaction has an early and asynchronic transition state, **H_2el. TS** (see Fig. 6). At the TS, only Al1-H_b increases moderately relative to that in the reactant, by 0.14-0.16 Å, whereas Al1-H_a actually decreases somewhat, with a hydrogen molecule (H_a-H_b) formed as described by H_a-H_b distance of 1.10-1.18 Å and corresponding imaginary frequency values of 644-751i cm^{-1}.

Figure 7 summarizes the profiles of ΔH(298.15 K) for the three unimolecular fragmentations of $Al_4H_{14}^-$ (**S3**) considered, with the corresponding ΔG(298.15 K) values given therein in parentheses. The most significant feature of these profiles is that there is only a tiny enthalpic/free energy barrier for H_2 loss, being 0.5/0.1 kcal mol^{-1}, suggesting that this elimination is remarkably facile (see also Table 4). This result, combined with the exothermicity of the process predicted for **S3** by 18 kcal mol^{-1} in terms of ΔH(298.15 K) and by 25 kcal mol^{-1} in terms of ΔG(298.15 K) suggests the $Al_4H_{14}^-$ cluster to be best described as a metastable species in the gas phase.

Table 4 Barrier height (kcal mol^{-1}) for the reaction of H_2 elimination from $Al_4H_{14}^-$(**S3**) calculated at the various computational levels

aug-cc-pVTZ[a]			G4[b]		
UB3LYP	UMP2	UCCSD(T)	ΔH(0 K)	ΔH(298.15 K)	ΔG(298.15 K)
0.3	0.2	0.5	0.5	0.5	0.1

[a] At the geometries calculated with each method, except for the UCCSD(T) value computed at the UMP2/aug-cc-pVTZ optimized structure

[b] ΔH (298.15 K) enthalpies and ΔG(298.15 K) free energies were calculated at the 1 atm and 298.15 K using the vibrational frequencies evaluated at the UB3LYP/GTBas3 level [14]; ΔH (0 K) enthalpy refers to T=0 K

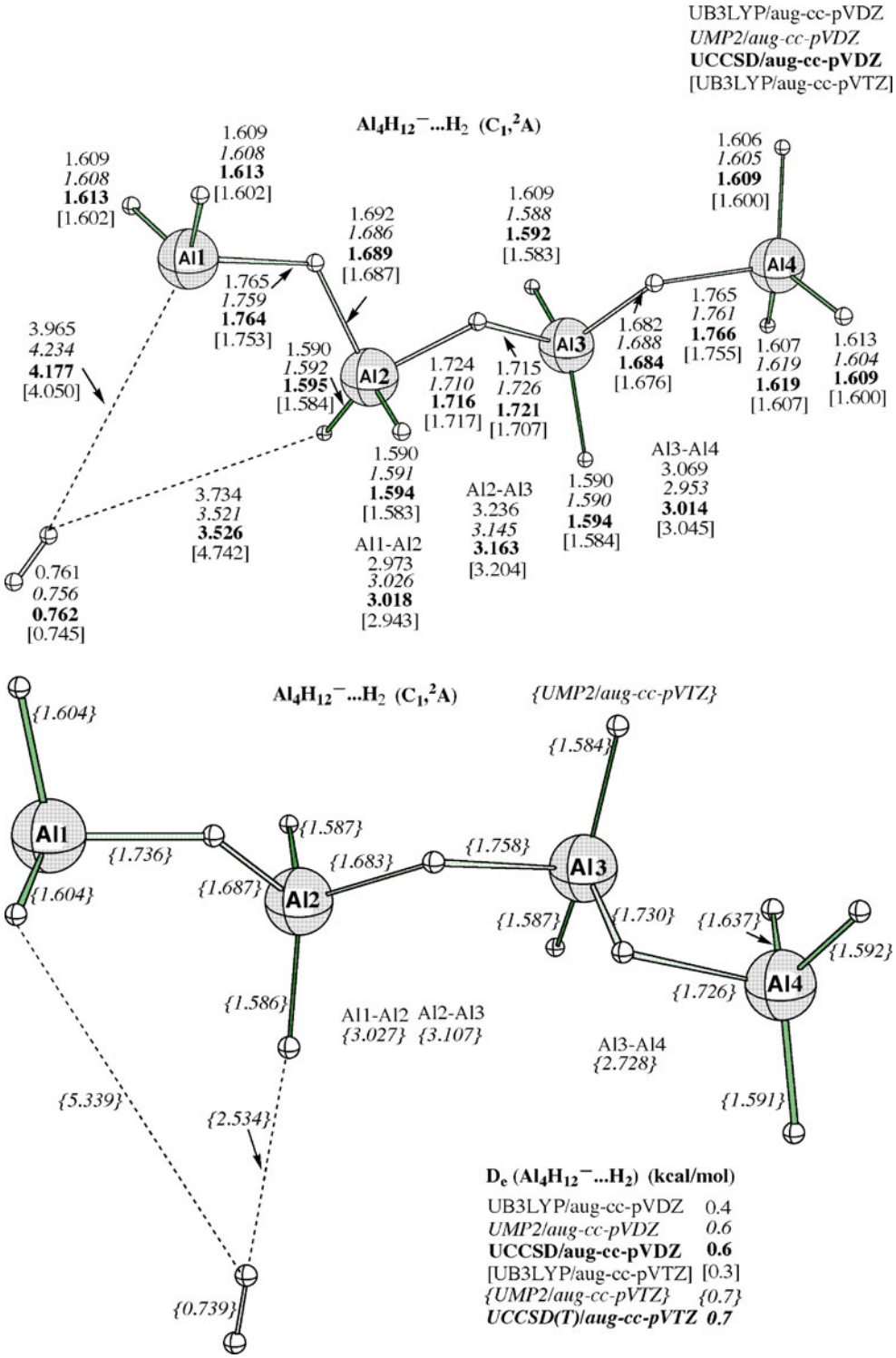

Fig. 8 A structure (distances in Ångstroms) and binding energy (D_e, kcal mol^{-1}) of the complex $Al_4H_{12}^-\ldots H_2$; D_e has been calculated as $[E(Al_4H_{12}^-)+E(H_2) - E(Al_4H_{12}^-\ldots H_2)]$

The post-reaction van der Waals complex between $Al_4H_{12}^-$ and H_2 has also been identified as reported in Fig. 8. This complex, denoted $Al_4H_{12}^-\ldots H_2$, was optimized at all five computational levels. Figure 8 shows that both the actual position of the H_2 subsystem within the complex and interaction distance(s) are method dependent. With UMP2/aug-cc-pVTZ, describing best long-range dispersion (at the optimization level), the complex has a structure in which the hydride fragment (Al_2-H) of $Al_4H_{12}^-$ interacts with the slightly polarized H-H bond (based on the Mulliken charges). Furthermore, the UMP2/aug-cc-pVTZ calculated interacting distance of 2.53 Å is distinctly reduced relative to those predicted with the other methods. The UCCSD(T)/aug-cc-pVTZ//UMP2/aug-cc-pVTZ binding energy (D_e) of

Table 5 The VDE energies (eV) of the **S1**, **S2**, **S3** and **S3′** structures of $Al_4H_{14}^-$ calculated a the UCCSD(T)/aug-cc-pVTZ//UMP2/aug-cc-pVTZ level[a]

S1	S2	S3	S3′
4.83	5.23	4.72	4.77

[a] The vertical detachment energy (VDE) was computed as the energy difference between the Al_4H_{14} neutral and $Al_4H_{14}^-$ anion at the anion optimized geometry

$Al_4H_{12}^-\ldots H_2$ amounts to 0.7 kcal mol^{-1}. Note that this value coincides with the UMP2/aug-cc-pVTZ result indicating the adequate description of dispersion already at the latter level (for comparison of the six D_e values of $Al_4H_{12}^-\ldots H_2$, see lower panel in Fig. 8).

VDE energies

The VDE energies of the four hydride structures of the $Al_4H_{14}^-$ anion computed at the UCCSD(T)/aug-cc-pVTZ//UMP2/aug-cc-pVTZ level are compared in Table 5. For the **S1**, **S2**, **S3** and **S3′** species the respective values are 4.83, 5.23, 4.72 and 4.77 eV. These VDEs are found to be even larger than the (adiabatic) electron detachment energy of the $Al_2H_7^-$ anion discussed above. On the other hand, except for the **S2** result, the remaining three VDEs are quite similar and might not help to assist in the future assignment of the actual isomer of the $Al_4H_{14}^-$ anion .

Does $Ga_4H_{14}^-$ galane exist?

Following the earlier work on comparing the structures, stabilities and bonding of the hydrogenated aluminum and gallium clusters [7], we next studied computationally $Ga_4H_{14}^-$ cluster anion. Although at the all-electron DFT UB3LYP/aug-cc-pVTZ level we located the $Ga_4H_{14}^-$ minimum analogue of $Al_4H_{14}^-$ (**S3**) (Fig. 9), neither our UB3LYP/ECP optimization nor that using the correlated UMP2/ECP method confirmed this result (the last two approaches employed the relativistic effective core potential ECP10MDF, see the footnote under Fig. 9). Similarly, our attempts to optimize the $Ga_4H_{14}^-$ counterparts of **S1** and **S2** led instead to the van der Waals complex $Ga_4H_{12}^-\ldots H_2$, depicted in Fig. 10. As in $Al_4H_{12}^-\ldots H_2$, the location of H_2 unit within $Ga_4H_{12}^-\ldots H_2$ and intermolecular separation are method dependent. Expectedly, the shortest separation between $Ga_4H_{12}^-$ and H_2 is calculated with UMP2/aug-cc-pVDZ and UMP2/ECP (the highest correlated optimization levels used for the complex). At the former geometry, the UCCSD(T)/aug-cc-pVTZ binding energy (D_e) of $Ga_4H_{12}^-\ldots H_2$ is 1.3 kcal mol^{-1} (see the lower panel in Fig. 10). As Fig. 10 shows additionally, the use of the relativistic ECP resulted in a significant shortening of the terminal Ga-H bonds compared to the all-electron results (this is actually a joint ECP/basis set effect).

The differences noticed here between the $Al_4H_{14}^-$ and $Ga_4H_{14}^-$ cluster anions are consistent with our recent symmetry-adapted perturbation theory (SAPT) analysis of the aluminum and gallium species pointing out to much stronger "hydride" character of the former [24]. The larger propensity of Al atom for hypercoordinate bonding situations compared to Ga [25] is a relevant qualitative explanation.

Conclusions

For the first time, distinct minima structures of the hydrogen-rich alane $Al_4H_{14}^-$, experimental observation of which was recently reported [6], have been identified at the correlated *ab*

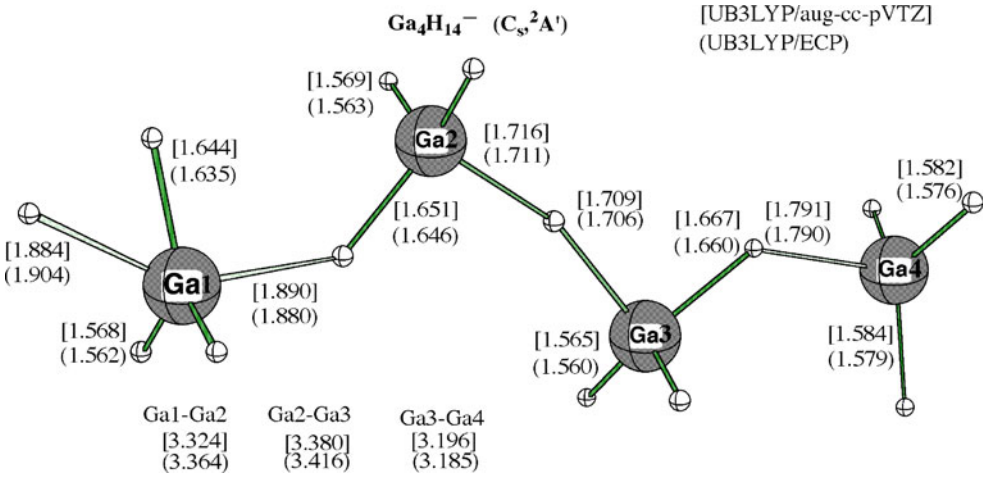

Fig. 9 A structure of the $Ga_4H_{14}^-$ analogue of $Al_4H_{14}^-$(**S3**) (distances in Ångstroms) calculated at the UB3LYP/aug-cc-pVTZ and UB3LYP/ECP levels. This structure appeared to be a minimum only with the all electron UB3LYP/aug-cc-pVTZ. No $Ga_4H_{14}^-$ minimum has been identified with either UB3LYP/ECP (the first-order saddle point with the imaginary frequency of 40i cm^{-1} was obtained at this level with the stringent optimization criteria and 'ultrafine' grid) or UMP2/ECP (H dissociation occurred from Ga1 during optimization)

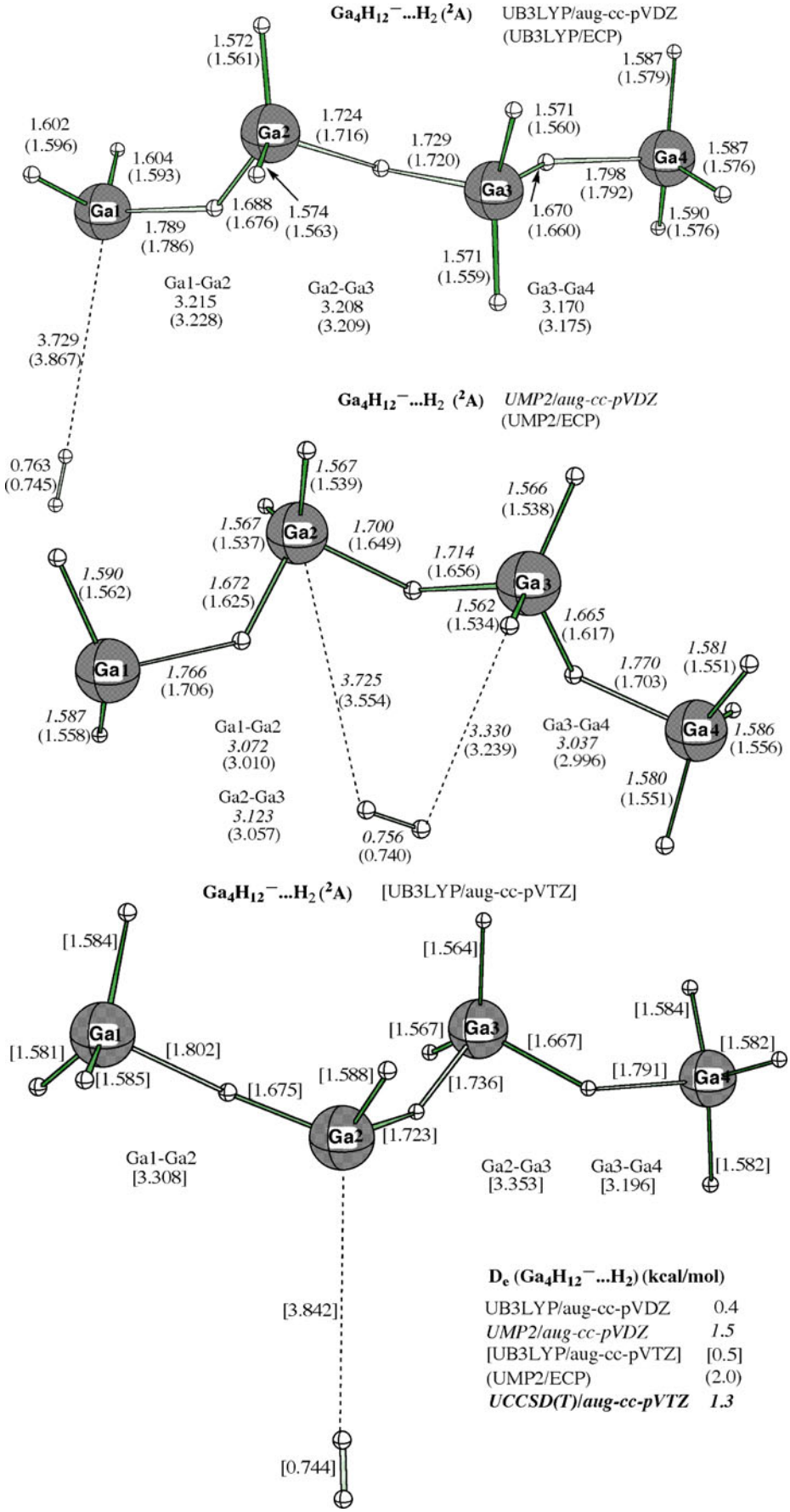

Fig. 10 A structure (distances in Ångstroms) and binding energy (D_e, kcal mol^{-1}) of the complex $Ga_4H_{12}^{-}\ldots H_2$ calculated at the all-electron and ECP levels; D_e has been calculated as $[E(Ga_4H_{12}^{-})+E(H_2) - E(Ga_4H_{12}^{-}\ldots H_2)]$ - note that the UCCSD(T)/aug-cc-pVTZ value of D_e has been computed at the UMP2/aug-cc-pVDZ optimized structures

initio levels, and thermodynamic and kinetic stability of this species was assessed at T=0 K and T=298.15 K. The structures found are chain-like, contain the multiple-coordinate Al center and approximately comprise the $Al_2H_7^-$ and Al_2H_7 moieties. Locating computationally some of the $Al_4H_{14}^-$ minima on the UCCSD and UMP2 potential energy surfaces required the triple-zeta quality basis set to describe adequately the Al multi-coordinate bonding. The dissociation of $Al_4H_{14}^-$ into the $Al_2H_7^-$ and Al_2H_7 units is predicted to require 20-22 (10-13) kcal mol^{-1} with ΔH(298.15 K) (ΔG(298.15 K)). However, $Al_4H_{14}^-$ is predicted to be metastable, because H_2 loss from its most favorable **S3** isomer is exothermic by 18 kcal mol^{-1} in terms of ΔH(298.15 K) and by 25 kcal mol^{-1} in terms of ΔG(298.15 K), with the enthalpic/free energy barrier involved being less than 1 kcal mol^{-1}. The global minimum on the $Al_4H_{14}^-$ anion energy surface corresponds to the weakly bound complex $Al_4H_{12}^-\ldots H_2$. This kind of complex appeared to be the only minimum structure identified for the gallium counterpart $Ga_4H_{14}^-$, when Ga relativistic effective core potential was used.

In the original experimental study, Li et al. [6] reported that they could observe strong $Al_nH_m^-$ intensities for m>3n "under some source conditions". Our current thermodynamic and kinetic (fragmentation reaction barrier) considerations suggest that due to the predicted $Al_4H_{14}^-$ metastability in the gas phase, this ion would in fact be detected only under the special experimental conditions.

Acknowledgments The author gratefully acknowledges computational resources provided by the Wroclaw Centre for Networking and Supercomputing, WCSS.

References

1. Li X, Grubisic A, Stokes ST, Cordes J, Ganteför GF, Bowen KH, Kiran B, Willis M, Jena P, Burgert R, Schnöckel H (2007) Science 315:356–358
2. Roach PJ, Reber AC, Woodward WH, Khanna SN, Castleman AW Jr (2007) Proc Natl Acad Sci USA 104:14565–14569
3. Grubisic A, Li X, Stokes ST, Cordes J, Ganteför GF, Bowen KH, Kiran B, Jena P, Burgert R, Schnöckel HJ (2007) J Am Chem Soc 129:5969–5975
4. Bazyn T, Krier H, Glumac N, Wang X, Jackson TL (2007) J Prop Power 23:457–464
5. Henke P, Huber M, Steiner J, Bowen KH, Eichhorn B, Schnöckel H (2009) J Am Chem Soc 131:5698–5704
6. Li X, Grubisic A, Bowen KH, Kandalam AK, Kiran B, Gantefoer GF, Jena P (2010) J Chem Phys 132:241103–241104
7. Moc J, Bober K, Mierzwicki K (2006) Chem Phys 327:247–260
8. Pople JA, Head-Gordon M, Raghavachari K (1987) J Chem Phys 87:5968–5975
9. Møller C, Plesset MS (1934) Phys Rev 46:618–622
10. Dunning TH (1989) J Chem Phys 90:1007–1023
11. Woon DE, Dunning TH (1993) J Chem Phys 98:1358–1371
12. Becke AD (1993) J Chem Phys 98:5648–5652
13. Lee C, Yang W, Parr RG (1988) Phys Rev B 37:785–789
14. Curtiss LA, Redfern PC, Raghavachari K (2007) J Chem Phys 126:084108–084112
15. Metz B, Stoll H, Dolg M (2000) J Chem Phys 113:2563–2569
16. Peterson KA (2003) J Chem Phys 119:11099–11112
17. Kendall RA, Dunning TH, Harrison RJ (1992) J Chem Phys 96:6796–6806
18. Frisch MJ et al (2010) Gaussian 09, Revision B01. Gaussian Inc, Wallingford, CT
19. Turley JW, Rinn HW (1969) Inorg Chem 8:18–22
20. Cui YH, Wang JG, Xu W (2010) Nanotechnology 21:025702
21. Chiles RA, Dykstra CE (1982) Chem Phys Lett 92:471–473
22. Charkin OP (2007) Russ J Inorg Chem 52:1925–1936
23. Goebbert DJ, Hernandez H, Francisco JS, Wenthold PG (2005) J Am Chem Soc 127:11684–11689
24. Moc J, Bober K, Panek J (2005) J Mol Model 12:93–100
25. Duke BJ, Liang C, Schaefer HF III (1991) J Am Chem Soc 113:2884–2890